Fakultät für Physik und
Astronomie
Universität Heidelberg

Bachelorarbeit im Studiengang Physik
angefertigt von

Vivienne Leidel

geboren in Heidelberg
Tag der Abgabe: 09.09.2019

Laser scattering calculations in pair producing plasmas

Diese Bachelorarbeit wurde angefertigt von Vivienne Leidel

am Max-Planck Institut für Kernphysik in Heidelberg

unter der Betreuung von

Honorarprof. Dr. Keitel

Abstract

The goal of this bachelor thesis is to investigate the laser scattering in a pair producing plasma with consideration of the radiation reaction. This is done for different parameters of a_0 and density as well as for different polarisations.

Zusammenfassung

Ziel dieser Bachelorarbeit ist es, die Laser-Streuung in einem Paar erzeugendem Plasma unter Berücksichtigung der Strahlungsrückwirkung zu untersuchen. Es wurden unterschiedliche Parameter a_0 und Dichten, sowie unterschiedliche Polarisationen berücksichtigt.

Contents

1 Introduction

In recent years, there has been tremendous progress in the goal towards producing ultra-intense laser pulse system. This quest for increasing higher laser intensities got further boost with the Extreme Light Infrastructure (ELI) project, where first tests produced an ultra-short laser pulse of 10 PW [1]. This opens up a whole new regime of laser-plasma interaction which is to be investigated. This is not only exiting for the point of view of fundamental research in physics, but it will also have a huge impact on medical physics, laser fusion, particle accelerators and astrophysics[2, 3, 4]. From the fundamental physics point of view, at such intensities the radiation reaction and quantum electrodynamics (QED) effects (like for example pair production) become significant. Investigating the radiation reaction force and pair-production from laser-plasma interaction has recently becomes a major area of research and not only it provides a fundamental test for the validity of QED, but it also it can lead to several new applications as mentioned before.

One of the topics that has recently gained attention is the electromagnetic cascade induced in the collision of two ultra-intense (I_l=10^{24}W/cm^2) laser pulses of linear polarisations. In this set-up, two linear polarized laser pulse collide to form a standing wave in the interaction region. Once an electron is injected into the focus of the interaction region of two laser pulse, this electron can gain energy and emit high-energy (GeV) photons. The interaction of these GeV photons with the laser pulse can produce a copious number of electron-positron pairs via the Breit-Wheeler process. This whole scenario is usually described as electromagnetic cascade and it has been extensively investigated in different settings [5, 6]. Usually in these works, the effect of the pair-plasma on the laser pulse is only discussed in terms of the energy-depletion of the laser pulse into high-energy photons and pairs. The

generated plasma can also cause a scattering of the laser pulse hindering the pair-production and electromagnetic cascades. This scattering is truly a manifestation of the plasma back-reaction on the laser pulse and it has not been studied in the literature so-far.

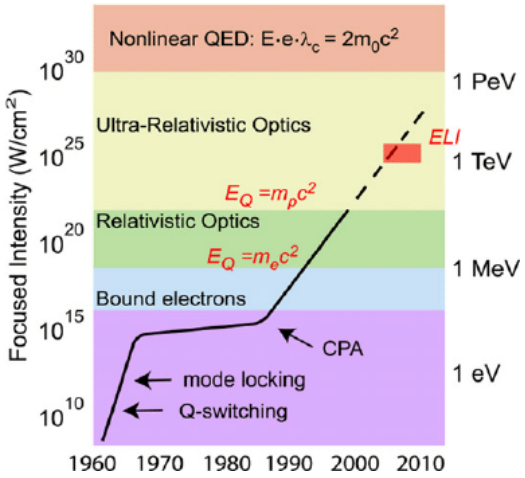

Fig. 1: Laser intensity development over time. ELI will address the ultra-relativistic regime with a_0 , $100 < a_0 < 10^4$. [7]

The purpose of this thesis is to systematically study the laser pulse scattering due to pair-production in an electron-ion plasma. Though, this configuration is not exactly the same as in electromagnetic cascades but it is closer to it and represents a first-step in this direction. The first part of the thesis focuses on the theoretical calculations of the dispersion relation and the instability growth rate in an electron-ion plasma. The instability arises because of the non-uniform rate of pair-production across the laser wavefront. This can happen either due to fluctuations on the laser wavefront and due to stochastic nature of the quantum radiation reaction force and pair-production, which is usually incorporated in PIC codes via a Monte Carlo method. The last part of this thesis is about simulations using a Particle-in-Cell (PIC) code. We employ laser pulse with different intensities, spatiotemporal profiles and polarisations at different plasma densities.

2 Theoretical prelude

First, we briefly discuss the radiation reaction force and pair-production by Breit-Wheeler process in a laser field. Afterwards we proceed for calculating the scattering of the laser pulse in a pair-producing plasma.

2.1 Radiation Reaction

The equation of motion for an electron in an external electromagnetic field considering the Lorentz Force is given by:

$$m\dot{u}^{\alpha} = -eF^{\alpha\beta}u_{\beta}, \tag{2.1}$$

where m is the mass of an electron, e the charge of an electron, $u^{\alpha} = \gamma(1, \vec{v})$ is the four velocity of the charge, $\gamma^{-1} = \sqrt{1 - \frac{v^2}{c^2}}$, $F^{\alpha\beta} = \partial^{\alpha}A^{\beta} - \partial^{\beta}A^{\alpha}$ is the electromagnetic tensor and A^{α} is the magnetic vector potential. At high laser intensities the equation of motion gets modified by an additional term, which describes the radiation reaction.The radiation reaction force, or also known as Abraham–Lorentz force, is a recoil force on an accelerating charged particle. This force is caused by the particle himself. If the particle is accelerated, a momentum is transferred to the field, and thus from momentum balance, a reaction force must act on the charged particle. The radiation carries away energy, and therefore acts as a frictional force, changing the equation of motion. This force can be described by the Lorentz-Abraham-Dirac (LAD) equation.

$$m\dot{u}^{\alpha} = -eF^{\alpha\beta}u_{\beta} + m\tau_0[\ddot{u}^{\alpha} + \dot{u}^2u^{\alpha}], \tag{2.2}$$

where $\tau_0 = \frac{2e^2}{3mc^3}$ is a constant. [8, 9]

The problem with this equation is that even for no external field, the acceleration does not vanish. This fact causes an unphysical solution.
Later other models have been introduced depending on the field strength and the particle energy. Since the radiation loss, depending on the regimes, can occur smoothly or in brutal steps, with diffusive and stochastic consequences. When quantum electrodynamics (QED) effect are negligible (classical regime), the radiation reaction can be treated as a continuous friction force acting on the particles. For this situation the Landau-Lifshitz equation can be applied. The equation is corresponding to the LAD up to first order of τ_0 and has no problem of unphysical properties[9].

$$\begin{aligned} m\dot{u}^\alpha =& - eF^{\alpha\beta}u_\beta - e\tau_0 \left\{ \frac{\partial F^{\alpha\beta}}{\partial x^\gamma} u_\beta u^\gamma - \frac{e}{m}\left[F^{\alpha\beta}F_{\beta\gamma}u^\gamma - F^{\beta\gamma}F_{\gamma\delta}u^\delta u_\beta u^\alpha \right] \right\} \\ =& \frac{2e^3\gamma}{3m_e c^3}\left\{ \left(\frac{\partial}{\partial t} + (v\cdot\nabla) \right) E + \frac{1}{c}\left[v \times \left(\frac{\partial}{\partial t} + (v\cdot\nabla) \right) B \right] \right\} \\ &+ \frac{2e^4}{2m_e^2 c^4}\left\{ E\times B + \frac{1}{c} B\times(B\times v) + \frac{1}{c}E(v\cdot E) \right\} \\ &- \frac{2e^4\gamma^2}{3m_e^2c^5} v \left\{ \left(E + \frac{1}{c} v\times B \right)^2 - \frac{1}{c^2}(v\cdot E)^2 \right\}. \end{aligned} \tag{2.3}$$

2.2 Pair generation

In this ultra-relativistic regime of laser-plasma interaction, not only the radiation reaction force but also also pair production is important. For pair production high energy photons are needed. The actual pair production process is the Breit-Wheeler process:

$$\gamma + n\omega \rightarrow e^- + e^+$$

where γ is a photon, ω the energy and e^-/e^+ an electron/positron.

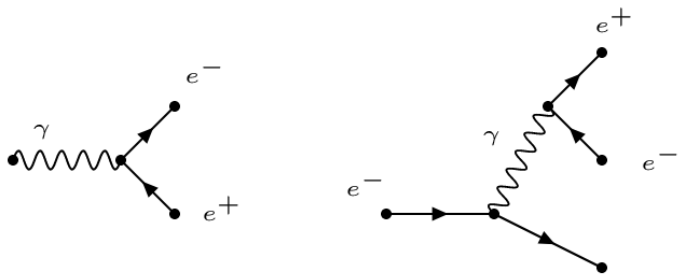

Fig. 2: Feynman diagrams of both processes

The nonlinear Breit-Wheeler effect occures when a high-energy photon decays into a pair of electron-positron while interacting with a strong electromagnetic field. In case of Breit-Wheeler the photon must first travel some distance before it produces a pair (in average a few laser wavelengths). There is also a two step process, Trident, which can be mentioned in case of pair production:

$$e^- \rightarrow 2e^- + e^+$$

First part is a nonlinear Compton scattering after which we have an electron and a photon. The second part is a nonlinear Breit-Wheeler process, where a photon decays into an electron-positron pair. In case of low laser intensity the Trident process dominates, but for higher intensity the Breit-Wheeler process becomes the dominant one.[10]

3 Laser scattering calculation

The instability of the laser pulse in a tenuous gas jet target were studied by different groups [11, 12]. The physical mechanism is as follows: due to uneven rate of ionization across the laser wavefront, there is a plasma density modulation which can scatter the laser. On scattering the density modulations get stronger causing further scattering and thus establishing a feedback loop. The instability vanishes as soon as the ionization is complete. Since the pair production is a stochastic event, uneven pair-production across the laser front can also cause the laser scattering. This can have consequences for the electromagnetic cascade proposed to be studied experimentally once ELI lasers are operational. To describe the radiation reaction we choose the Landau-Lifshitz equation since we consider to be in the classical electrodynamics regime, i.e quantum effects are negligible (spin, photon recoil), and further more $\lambda_c << \lambda$ and $E << E_{cr}$ [8] apply. Where λ_c is the Compton wavelength and E_{cr} the critical field of the quantum electrodynamics.

3.1 Equation of motion

We begin with a circular polarised laser pulse propagating in $\hat{z}$ direction in an electron-ion plasma. This laser is strong enough to cause pair-production which we include in the form of a rate equation. The most common method to describe a plasma is using the two fluid model.

Our considered plasma consists of ions and electrons. Since we assume that there is no ionization or recombination between the electrons and ions and we assume a collisionless plasma (collisions can be neglected since the mean free path between particles is larger than the wavelength of the oscillations in the plasma), the continuity

equation must be fulfilled for the phase space distribution function $f(x, v, t)$:

$$\frac{df}{dt} = \frac{\partial f}{\partial t} + \frac{\partial}{\partial x} \cdot (\dot{x} f) + \frac{\partial}{\partial v} \cdot (\dot{v} f) = 0. \tag{3.1}$$

With additionally the equation of motion:

$$\begin{aligned} \dot{x} &= v, \\ \dot{v} &= \frac{q}{m} \left(E + \frac{v \times B}{c} \right). \end{aligned} \tag{3.2}$$

This leads to the Vlasov equation:

$$\frac{\partial f}{\partial t} + v \cdot \frac{\partial f}{\partial x} + \frac{q}{m} \left(E + \frac{v}{c} \times B \right) \frac{\partial f}{\partial v} = 0, \tag{3.3}$$

with the magnetic field B, the electric field E as well as the charge q and the mass m of the particle.

For our case, we modify the Vlasov equation by considering additionally the radiation reaction and taking the phase space distribution $p(x, t)$.

$$\dot{v} = \frac{q}{m} \left(E + \frac{v \times B}{c} \right) + \frac{2e^4}{3m^2c^5} \gamma^2 v \left[\left(E + \frac{1}{c} v \times B \right)^2 - \left(\frac{v}{c} E \right)^2 \right]. \tag{3.4}$$

Here only the leading order term of the radiation reaction 2.3 is included. The other terms of the radiation reaction are smaller by $1/\gamma << 1$ and thus can be ignored. This leads to an equation of motion of

$$\frac{dp}{dt} + v \cdot \nabla p = -e \cdot (E + v \times B) - \frac{2e^4}{3m^2c^5} \gamma^2 v \left[\left(E + \frac{1}{c} v \times B \right)^2 - \left(\frac{v}{c} E \right)^2 \right]. \tag{3.5}$$

We can rewrite this in potential form using $E = -\frac{1}{c} \frac{\partial A}{\partial t} - \nabla \phi$ and $B = \nabla \times A$ for an pulse of the form

$$A = \frac{1}{2}A_\perp(x_\perp, z, t)e^{ik_0 z - iw_0 t} + cc., \tag{3.6}$$

with slow varying amplitude

$$\left|\frac{\partial A_\perp}{\partial t}\right| << |w_0 A_\perp|, \ \left|\frac{\partial A_\perp}{\partial z}\right| << |k_0 A_\perp|. \tag{3.7}$$

If we further more consider the transverse variation to be weak compared to the laser wavelength, i.e. $k_\perp << k_0$, than the equation of motion can be rewritten as:

$$\begin{aligned}\frac{dp}{dt} + v\cdot\nabla p =& \frac{e}{c}\frac{\partial A}{\partial t} + e\nabla\phi - \frac{e}{c}\left(v\times(\nabla\times A)\right) \\ &- \frac{2e^4 w_0^2}{3m^2c^7}\gamma^2 v\left[\left(A + \frac{v}{c}\times(\hat{e}_z\times A)\right)^2 - \left(\frac{v}{c}A\right)^2\right].\end{aligned} \tag{3.8}$$

Initially we can ignore the radiation reaction term (second row) and solve for $p_\perp$. Without the radiation reaction force the perpendicular component of the moment could be written as

$$p_\perp = \frac{e}{c}A. \tag{3.9}$$

A purely transverse circular polarised light in plasmas is only possible when we ignore the z-component of motion, i.e. purely transverse circular polarised light doesn't induce motion in z direction. Now we simplify the radiation reaction term using the above expression for the transverse momentum. The radiation reaction term then becomes:

$$\begin{aligned}&\frac{2e^4 w_0^2}{3m^2c^7}\gamma^2 v\left[\left(A + \frac{v}{c}\times(\hat{e}_z\times A)\right)^2 - \left(\frac{v}{c}A\right)^2\right] \\ &= \frac{2e^4 w_0^2}{3m^2c^7}\gamma^2\frac{p_\perp}{m\gamma}\left[\left(\left(\frac{v}{c}\cdot A\right)\hat{e}_z - \left(\frac{v}{c}\cdot\hat{e}_z\right)A + A\right)^2 - \left(\frac{v}{c}A\right)^2\right] \\ &= \frac{2e^4 w_0^2}{3m^2c^7}\gamma|A|^2 p_\perp.\end{aligned} \tag{3.10}$$

Using 3.9 γ can be written as

$$\gamma = (1 + e^2A^2/m^2c^4)^{1/2}. \tag{3.11}$$

Now we can solve the equation of motion perturbatively using the simplified expression for the radiation reaction force. Which results to:

$$\frac{\partial}{\partial t}\left(p_\perp - \frac{e}{c}A\right) = -\frac{2e^4w_0^2}{3m^2c^7}\gamma|A|^2p_\perp, \tag{3.12}$$

this can be solved to

$$p_\perp = -\frac{2e^4w_0^2}{3m^2c^7}\gamma|A|^2\int_0^t \frac{e}{c}A\ dt + \frac{e}{c}A = \frac{e}{c}A + \frac{2e^4w_0^2}{3m^2c^7}\gamma|A|^2\frac{e}{c}\frac{A}{iw_0} = \frac{e}{c}A(1 - i\alpha\gamma|A|^2), \tag{3.13}$$

where $\alpha = 2e^4w_0/3m^3c^7$. As we can see, the radiation reaction yields to an additional term which has a relative minus sign, signaling the frictional nature.

3.2 Wave equation

For further analysis we must take into account the wave equation for the electromagnetic vector potential. Starting with the Maxwell equation

$$\nabla \times B = \frac{4\pi}{c}J - \frac{1}{c}\frac{\partial E}{\partial t}. \tag{3.14}$$

We substitute for E and B the potential form and choosing the Lorenz gauge:

$$\frac{1}{c^2}\frac{\partial^2 A}{\partial t^2} - \nabla^2 A = \frac{4\pi}{c}J - \frac{1}{c}\frac{\partial}{\partial t}\nabla\phi. \tag{3.15}$$

Considering the Poisson equation $\nabla^2\phi = -4\pi\rho$ and the equation of charge conservation

$\frac{\partial \rho}{\partial t} + \nabla J = 0$ where ρ is the charge density, we will get:

$$\nabla \left(\frac{\partial}{\partial t} \nabla \phi - 4\pi J \right) = 0. \tag{3.16}$$

To get rid of the $\nabla\phi$ the current density J can be separated in a transverse part J_t and a longitudinal part J_l. Since $\nabla J_t = 0$ we obtain $\frac{\partial}{\partial t}\nabla\phi = 4\pi J_l$ with $J_t = -n_e e v_\perp = -n_e \frac{e^2}{mc\gamma} A(1 - i\alpha\gamma|A|^2)$ (if we restrict ourselves to $A \cdot \nabla n_e = 0$) and where the electron density is $n_e = n_0 + 2n_{ep}$

$$\nabla^2 A - \frac{1}{c^2}\frac{\partial^2 A}{\partial t^2} = \frac{4\pi n e^2}{m\gamma c^2}\left(1 - i\alpha\gamma|A|^2\right)\left(1 + \frac{2n_{ep}}{n_0}\right) A, \tag{3.17}$$

where n_0 is the equilibrium plasma electron density and n_{ep} is the density of the pair particles. The factor of two is due to the pair production.

$$\frac{\partial n}{\partial t} = R(n_0 + 2n_{ep}). \tag{3.18}$$

Here R is the rate of pair production due to either of the previous mentioned pair production processes. This equation is suited for both processes since the spacial growth of the instability should be larger than the distance a photon needs to create a pair.

For the instability analysis it is more convenient to change to the laser frame coordinates $\xi = ct - z$, $\eta = z$. The variable ξ measures the distance back from the head of the pulse, as the pulse propagates in the positive z direction. This changes the derivation according to:

$$\frac{\partial}{\partial t} = \frac{\partial}{\partial \xi}\frac{\partial \xi}{\partial t} + \frac{\partial}{\partial \eta}\frac{\partial \eta}{\partial t} = c\frac{\partial}{\partial \xi}, \tag{3.19}$$

$$\frac{\partial}{\partial z} = \frac{\partial}{\partial \xi}\frac{\partial \xi}{\partial z} + \frac{\partial}{\partial \eta}\frac{\partial \eta}{\partial z} = \frac{\partial}{\partial \eta} - \frac{\partial}{\partial \xi}, \tag{3.20}$$

$$\frac{\partial^2}{\partial t^2} = c^2 \frac{\partial^2}{\partial \xi^2}, \tag{3.21}$$

$$\begin{aligned} \frac{\partial^2}{\partial z^2} = \frac{\partial}{\partial z}\left(\frac{\partial}{\partial z}\right) &= \left(\frac{\partial}{\partial \eta} - \frac{\partial}{\partial \xi}\right)\left(\frac{\partial}{\partial \eta} - \frac{\partial}{\partial \xi}\right) \\ &= \frac{\partial^2}{\partial \eta^2} - 2\frac{\partial}{\partial \xi}\frac{\partial}{\partial \eta} + \frac{\partial^2}{\partial \xi^2}. \end{aligned} \tag{3.22}$$

In the new coordinates A becomes $A = \frac{1}{2}A_\perp e^{ik_o\xi} + cc.$ and the derivatives change to

$$\frac{\partial A}{\partial \xi} = \frac{1}{2}\left[\frac{\partial A_\perp}{\partial \xi} - ik_0 A_\perp\right] e^{-ik_0\xi}, \tag{3.23}$$

$$\begin{aligned} \frac{\partial^2 A}{\partial \xi^2} &= \frac{1}{2}\frac{\partial}{\partial \xi}\left[\frac{\partial A_\perp}{\partial \xi} - ik_0 A_\perp\right] e^{-ik_0\xi} \\ &= \frac{1}{2}\left[\frac{\partial^2 A_\perp}{\partial \xi^2} - 2ik_0\frac{\partial A_\perp}{\partial \xi} - k_0^2 A_\perp\right] e^{-ik_0\xi}. \end{aligned} \tag{3.24}$$

This changes the wave equation 3.17 to:

$$\nabla_\perp^2 A_\perp + \frac{\partial^2 A_\perp}{\partial \eta^2} - 2\frac{\partial}{\partial \xi}\frac{\partial A_\perp}{\partial \eta} + \frac{\partial^2 A_\perp}{\partial \xi^2} - \frac{\partial^2 A_\perp}{\partial \xi^2} = \frac{4\pi n e^2}{m\gamma c^2}\left(1 - i\alpha\gamma|A|^2\right)\left(1 + \frac{2n_{ep}}{n_0}\right)A_\perp, \tag{3.25}$$

$$\nabla_\perp^2 A_\perp + \frac{\partial^2 A_\perp}{\partial \eta^2} + 2\frac{\partial}{\partial \eta}\left[ik_0 - \frac{\partial}{\partial \xi}\right]A_\perp = \frac{4\pi n e^2}{m\gamma c^2}\left(1 - i\alpha\gamma|A|^2\right)\left(1 + \frac{2n_{ep}}{n_0}\right)A_\perp. \tag{3.26}$$

With $A_\perp$ slowly varying in η this leads to:

$$\nabla^2 A_\perp + 2\frac{\partial}{\partial \eta}\left[ik_0 - \frac{\partial}{\partial \xi}\right]A_\perp = \frac{4\pi n e^2}{m\gamma c^2}\left(1 - i\alpha\gamma|A|^2\right)\left(1 + \frac{2n_{ep}}{n_0}\right)A_\perp, \tag{3.27}$$

$$\nabla_\perp^2 A_\perp + 2\frac{\partial}{\partial \eta}\left[ik_0 - \frac{\partial}{\partial \xi}\right]A_\perp = \frac{w_p^2}{\gamma c^2}\left(1 - i\alpha\gamma\frac{|A_\perp|^2}{2}\right)\left(1 + \frac{2n_{ep}}{n_0}\right)A_\perp. \tag{3.28}$$

Due to the new coordinates the rate equation changes to:

$$c\frac{\partial n_{ep}}{\partial \xi} = R(n_0 + 2n_{ep}). \tag{3.29}$$

The laser scattering leads to a vector potential of :

$$A_\perp = A_0 + \delta A_+ e^{ik_\perp x_\perp} + \delta A_-^* e^{-ik_\perp x_\perp}, \tag{3.30}$$

with $\delta A_{+/-}$ being an up-/downshifted perturbation. The density perturbation takes the form

$$\frac{n_{ep}}{n_0} = n_{p0} + \delta n_+ e^{ik_\perp x_\perp} + \delta n_-^* e^{-ik_\perp x_\perp}. \tag{3.31}$$

To deduce the new rate of pair production linearize it to:

$$R\left(|A_0 + \delta A_+ e^{ik_\perp x_\perp} + \delta A_-^* e^{-ik_\perp x_\perp}|\right) = R\left(|A_0|\right) + \frac{\partial R}{\partial |A_0|}\frac{A_0^*\delta A_+ + A_0^*\delta A_-}{2|A_0|}e^{ik_\perp x_\perp} + cc., \tag{3.32}$$

with $w_p^2 = 4\pi n_0 e^2/m$. To further investigate 3.28 we must calculate all the involved terms. Resulting to:

$$|A_\perp|^2 = |A_0|^2 + (A_0^*\delta A_+ + A_0\delta A_-)e^{ik_\perp x_\perp} + (A_0\delta A_+^* + A_0^*\delta A_-^*)e^{-ik_\perp x_\perp}, \tag{3.33}$$

$$\frac{1}{\gamma} = \frac{1}{\gamma_0} - \frac{e^2}{4m^2c^4\gamma_0^3}[(A_0^*\delta A_+ + A_0\delta A_-)e^{ik_\perp x_\perp}] - \frac{e^2}{4m^2c^4\gamma_0^3}[(A_0\delta A_+^* + A_0^*\delta A_-^*)e^{-ik_\perp x_\perp}], \tag{3.34}$$

where $\gamma_0 = (1 + a_0^2/2)^{1/2}$ and $a_o = eA_o/mc^2$

$$\frac{A_\perp}{\gamma} = \frac{A_0}{\gamma_0} + \left[\frac{\delta A_+}{\gamma_0} - \frac{a_0^2}{4\gamma_0^3}(\delta A_+ + \delta A_-)\right]e^{ik_\perp x_\perp} + \left[\frac{\delta A_-^*}{\gamma_0} - \frac{a_0^2}{4\gamma_0^3}(\delta A_+^* + \delta A_-^*)\right]e^{-ik_\perp x_\perp} + cc., \tag{3.35}$$

$$\begin{aligned}|A_\perp|^2 A_\perp =& |A_0|^2 A_0 + [|A_0|^2(\delta A_+ + \delta A_-) + |A_0|^2 \delta A_+] e^{ik_\perp x_\perp} \\ &+ [|A_0|^2(\delta A_+^* + \delta A_-^*) + |A_0|^2 \delta A_-^*] e^{-ik_\perp x_\perp} + cc.\end{aligned} \tag{3.36}$$

The now explicitly calculated part can be inserted in 3.28 and then separate in terms with the same phase. This can be done since the exponential function builds a basis. If we take a look at the equilibrium part it results to:

$$\nabla_\perp^2 A_0 + 2\frac{\partial}{\partial \eta}\left[ik_0 - \frac{\partial}{\partial \xi}\right] A_0 = \frac{w_p^2}{\gamma_0 c^2}(1 + 2n_{p0})(1 - i\psi a_0^2 \gamma_0) A_0, \tag{3.37}$$

since we neglected the time and space dependence of the equilibrium density distribution 3.37, the equilibrium field undergoes a small wave number shift due to the plasma [11]. Upon linearising A_0 as $\hat{A}_0 e^{i\delta k \eta}$ the wave number shift δk becomes

$$\delta k = -\frac{k_p^2 \Delta}{2k_0}(1 - i\psi a_0^2 \gamma_0), \tag{3.38}$$

where $k_p^2 = w_p^2/\gamma_0 c^2$, $\Delta = (1 + 2n_{p0})$, $\alpha = 2\psi e^2/m^2 c^4$, $\psi = r_e w_0/3c$ and $r_e = e^2/mc^2$. Collecting the terms involving $e^{\pm ik_\perp x_\perp}$ results to:

$$\begin{aligned}&\left[\nabla_\perp^2 + 2\frac{\partial}{\partial \eta}\left(ik_0 - \frac{\partial}{\partial \xi}\right)\right] \delta A_+ e^{\pm ik_\perp x_\perp} = \frac{w_p^2}{c^2}\Delta \left[\frac{\delta A_+}{\gamma_0} - \frac{a_0^2}{4\gamma_0^3}(\delta A_+ + \delta A_-)\right] e^{\pm ik_\perp x_\perp} \\ &+ k_p^2 \delta n_+ \left(1 - i\psi a_0^2 \gamma_0\right) A_0 e^{\pm ik_\perp x_\perp} - i\psi a_0^2 \frac{w_p^2}{c^2}\Delta \left[\delta A_+ + (\delta A_+ + \delta A_-)\right] e^{\pm ik_\perp x_\perp},\end{aligned} \tag{3.39}$$

$$\begin{aligned}&\left[\nabla_\perp^2 - k_p^2 \Delta\left(1 - i\psi a_0^2 \gamma_0\right) + 2\frac{\partial}{\partial \eta}\left(ik_0 - \frac{\partial}{\partial \xi}\right)\right] \delta A_+ e^{\pm ik_\perp x_\perp} = \\ &- \left(1 - 4i\psi\gamma_0^3\right)\frac{w_p^2}{c^2}\Delta \frac{a_0^2}{4\gamma_0^3}(\delta A_+ + \delta A_-) e^{\pm ik_\perp x_\perp} + k_p^2 \delta n_+ \left(1 - i\psi a_0^2 \gamma_0\right) A_0 e^{\pm ik_\perp x_\perp}.\end{aligned} \tag{3.40}$$

3.3 Calculation of the dispersion relation and growth rate

To further calculate the dispersion relation the density perturbation is needed. Similar instabilities derivations can also be found in the book from Kruer [13] and Gibbon [14]. This can be deduced using the density perturbation 3.31 and upon assuming $\delta n_+ \sim e^{-k_\xi \xi + i(k_\eta \pm \delta k)\eta}$ which then results to:

$$c\frac{\partial n_{ep}}{\partial \xi} = R(n_0 + 2n_{ep}), \tag{3.41}$$

$$c\frac{\partial \delta n_+}{\partial \xi} = R_0 \delta n_+ + \Delta \frac{\partial R}{\partial |A_0|}\frac{A_0^* \delta A_+ + A_0^* \delta A_-}{2|A_0|}, \tag{3.42}$$

$$\delta n_+ = -\frac{\Delta}{R_0 + ik_\xi c}\frac{\partial R}{\partial |A_0|}\frac{A_0^* \delta A_+ + A_0^* \delta A_-}{2|A_0|}. \tag{3.43}$$

Here we see that the perturbed electron density is coupled to the perturbed laser field through the dependence of the pair production rate on the equilibrium field. Using this expression and writing $\delta A_\pm$ as $\delta \hat{A}_\pm e^{-ik_\xi \xi + i(k_\eta \pm \delta k)\eta}$ corresponds to

$$[k_\perp^2 + 2k_\eta(k_\xi + k_0)]\delta A_+ = \left[\frac{k_p^2 \Delta |a_0|}{2(R_0 + ik_\xi c)}\frac{\partial R}{\partial |A_0|}(1 - i\psi a_0^2 \gamma_0) + \frac{w_p^2 \Delta a_0^2}{4\gamma_0^3 c^2}(1 + 4\psi\gamma_0^3)\right](\delta A_+ + \delta A_-). \tag{3.44}$$

For δA_- it results to

$$[k_\perp^2 + 2k_\eta(k_\xi + k_0)]\delta A_- = \left[\frac{k_p^2 \Delta |a_0|}{2(R_0 + ik_\xi c)}\frac{\partial R}{\partial |A_0|}(1 + i\psi a_0^2 \gamma_0) + \frac{w_p^2 \Delta a_0^2}{4\gamma_0^3 c^2}(1 - 4\psi\gamma_0^3)\right](\delta A_+ + \delta A_-). \tag{3.45}$$

With this we've got $D_+ \delta A_+ = R_+(\delta A_+ + \delta A_-)$ and $D_- \delta A_- = R_-(\delta A_+ + \delta A_-)$ yielding to the dispersion relation

$$\left(\frac{R_+}{D_+} + \frac{R_-}{D_-}\right) = 1, \tag{3.46}$$

where

$$D_{\pm} = k_{\perp}^2 + 2k_{\eta}(k_{\xi} \pm k_0), \tag{3.47}$$

$$R_{\pm} = \left[\frac{k_p^2 \Delta |a_0|}{2(R_0 + ik_{\xi}c)} \frac{\partial R}{\partial |A_0|} (1 \mp i\psi a_0^2 \gamma_0) + \frac{w_p^2 \Delta a_0^2}{4\gamma_0^3 c^2} (1 \pm 4i\psi\gamma_0^3 \right]. \tag{3.48}$$

In case of pair production the frequency gets upshifted, therefore we only retains the upshifted components of the dispersion relation. For this case it results to

$$k_{\perp}^2 + 2k_{\eta}(k_{\xi} + k_0) = \frac{\sigma_1}{R_0 + ik_{\xi}c}(1 - i\psi a_0^2\gamma_0) + \sigma_2(1 + 4i\psi\gamma_0^3). \tag{3.49}$$

The pole of this dispersion relation ($D_+ = 0$ and since $k_{\xi} << k_0$) is $k_{\eta} = -k_{\perp}/2k_0$ this leads to

$$D_+^u = \beta_G k_0 + k_{\eta} - \beta_G k_{\xi} - \frac{\sigma_1}{2k_0} \frac{(1 - i\psi a_0^2\gamma_0)}{R_0 + ik_{\xi}c} - \frac{\sigma_2}{2k_0}(1 + 4i\psi\gamma_0^3), \tag{3.50}$$

where

$$\beta_G = k_{\perp}^2/2k_0^2, \sigma_1 = \frac{k_p^2 \Delta a_0}{2} \frac{\partial R}{\partial |A_0|}, \sigma_2 = \frac{a_0^2 k_p^2 \Delta}{4\gamma_0^3}, \tag{3.51}$$

since $D_+^u = 0$

$$k_{\eta} = \beta_G(k_{\xi} - k_0) + \frac{\sigma_1}{2k_0} \frac{(1 - i\psi a_0^2\gamma_0)}{R_0 + ik_{\xi}c} + \frac{\sigma_2}{2k_0}(1 + 4i\psi\gamma_0^3). \tag{3.52}$$

We substitute $\hat{k}_{\eta} = k_{\eta} - \beta_{\xi} k_{\xi}$ in the dispersion relation and differentiating it with respect to k_{ξ} while keeping $\hat{k}_e ta$ constant. Which gives

$$(\beta_{\xi} - \beta_G) = -\frac{\sigma_1 ic}{2k_0} \frac{(1 - i\psi a_0^2\gamma_0)}{(R_0 + ik_{\xi}c)^2}, \tag{3.53}$$

$$k_{\xi} = \frac{iR_0}{c} \pm \sqrt{\frac{\sigma_1}{2k_0 c(\beta_{\xi} - \beta_G)}} \left[\frac{1+i}{\sqrt{2}} + \frac{1-i}{2\sqrt{2}} \psi a_0^2 \gamma_0 \right], \tag{3.54}$$

here $\psi a_0^2\gamma_0 << 1$ ($I_L \sim 10^{23}W/cm^2$) is assumed. The complex growth of the perturbation is

$$\Gamma = (k_\eta - \beta_\xi k_\xi)\eta + i\delta k_\eta. \tag{3.55}$$

With the involved terms written as

$$\begin{aligned}(k_\eta - \beta_\xi k_\xi) = &-\frac{iR_0}{c}(\beta_\xi - \beta_G) - \beta_G k_0 + \frac{\sigma_2}{2k_0}(1 + 4i\psi\gamma_0^3) \\ &\mp 2\sqrt{\frac{\sigma_1(\beta_\xi - \beta_G)}{2k_0 c}}\left[\frac{1+i}{\sqrt{2}} + \frac{(1-i)}{2\sqrt{2}}\psi a_0^2\gamma_0\right].\end{aligned} \tag{3.56}$$

This results to

$$\begin{aligned}\Gamma = &\left[\frac{R_0}{c}(\beta_\xi - \beta_G) - i\beta_G k_0 + \frac{i\sigma_2}{2k_0} - \frac{2\sigma_2\psi\gamma_0^3}{k_0} \pm \sqrt{\frac{\sigma_1}{k_0}(\beta_\xi - \beta_G)}\left((1-i) - \frac{(1+i)}{2}\psi a_0^2\gamma_0\right)\right]\eta \\ &- \frac{ik_p^2\Delta}{2k_0}\eta - \frac{k_p^2\Delta}{2k_0}\psi a_0^2\gamma_0\eta,\end{aligned} \tag{3.57}$$

leading to the final expression of

$$\begin{aligned}\Gamma = &\frac{R_0}{c}\left(\xi - \frac{k_\perp^2}{2k_0^2}\eta\right) - \frac{ik_\perp^2}{2k_0}\eta + \frac{ia_0^2k_p^2\Delta}{4\gamma_0^2}\eta - \frac{a_0^2k_p^2\Delta\psi\gamma_0}{2k_0}\eta \\ &\pm \sqrt{\frac{k_p^2\Delta a_0}{2k_0}\frac{\partial R}{\partial|A_0|}(\xi\eta - \frac{k_\perp^2}{2k_0^2}\eta^2)}\left[(1-i) - \frac{(1+i)}{2}\psi a_0^2\gamma_0\right] - \frac{ik_p^2\Delta}{2k_0}\eta - \frac{k_p^2\Delta}{2k_0}\psi a_0^2\gamma_0\eta.\end{aligned} \tag{3.58}$$

For long-term asymptote, $\xi \gg (k_\perp^2/2k_0^2)\eta$. From this equation we can clearly see that the growth rate of the instability depends both on the rate of the pair-production R_0 and the variation of rate of pair-production across the laser wavefront, $|\partial R/\partial A_0|$. Moreover, though a finite $k_\perp$ can provide a seed for the scattering, a larger value of $k_\perp$ reduces the growth rate. Thus, for a laser pulse of Gaussian profile, although the rate of pair-production can strongly vary across its wavefront, the scattering is weaker due to a larger $k_\perp$ in the early phase of the instability development. Also the

first term in the expression is independent of the plasma density confirming that pair-production alone causes the scattering. However, the term with $|\partial R/\partial A_0|$ depends on the plasma density. Thus, there is an optimum range where the scattering is maximum. Even though these calculations are valid only for the circularly polarised laser pulse, we expect the results to be qualitatively similar in the linear polarisation pulse case too.

4 PIC Simulations of the laser scattering

The code we used for the simulations is SMILEI [15], which is an open-source code for plasma simulations. It is written in C++ but the input file can be done in python. A short introduction to PIC algorithm can be found in Appendix A. We consider a scenario where an electron-ion plasma target is irradiated with a laser pulse. The ratio between the mass of the ion m_i and electron m_e is set to be $m_i/m_e = 1836$ corresponding to the ratio between a proton and an electron and the ion is charged $Z_i = 1$. The target starts after 6 μm of vacuum and is 50 μm long. The value of the plasma densities are chosen in such a way that plasma is relativistically transparent to the laser pulse. The input values can be found summarized in table 1.

simulation parameters	value
mass ratio m_i/m_e	1836
charge ion Z_i	1
Particles per cell	16
$L_x \times L_y[\mu m^2]$	128×8
$\Delta_x \times \Delta_y[nm^2]$	20×10
$T_{sim}[\mu m/c]$	380
$dt[nm/c]$	$6.\overline{6}$
$\lambda_0[\mu m]$	1
length vacuum $[\mu m]$	6
length target $[\mu m]$	50
photon threshold for RR	2
radiation reaction model	Monte Carlo

Tab. 1: constant simulation parameters

The above-mentioned values are kept constant for all simulations. The changes between the simulations occur in the density and the laser pulse.

In this thesis following simulations are included:

- planar linear polarised laser puls with $a_0 = 400$ and density of $50n_c$
- planar linear polarised laser puls with $a_0 = 400$ and density of $100n_c$
- planar linear polarised laser puls with $a_0 = 400$ and density of $420n_c$
- planar circular polarised laser puls with $a_0 = 400$ and density of $420n_c$
- Gaussian linear polarised laser puls with $a_0 = 420$ and density of $550n_c$
- Gaussian circular polarised laser puls with $a_0 = 350$ and density of $50n_c$

whereas $a_0 = eE_0/m_e\omega_0 c$ is the normalized vector potential, $n_c = m_e\omega_0^2/4\pi e^2$ the critical density of the laser pulse and ω_0 is the laser frequency.

In table 2 the parameters of the Gaussian puls can be found.

simulation parameters	value
focus	$[L_x/2, L_y/2]$
spacial waist$[\mu m]$	4
time fwhm	$T_{sim}/3$
duration	T_{sim}

Tab. 2: Gaussian profile

4.1 Shock formation

Before we discuss the laser scattering, we can briefly also discuss the shock formation by different laser pulse polarisations. As mentioned before, we expect the laser scattering to be qualitatively same for both polarisations. However, there is one crucial difference between the two polarisation cases. It is the shock formation and it's worthwhile to to briefly discuss before moving to the laser scattering. In Fig.3 and 4 we can see the shock formation in case of circular and linear polarised laser pulses, with and without radiation reaction at different time instances. To evaluate the shock formation we must take the number density of the plasma and divide it by the initial density. If this value gets larger than 3 it is considered to be a shock. The laser penetration in the target in case of RR is less in comparison with and no RR case. This is due to the energy lost in radiations that causes the laser piston to move slowly, consequently the shock structure is at earlier position than in no RR case. With RR the shock seems to have more structure in the front. We can also see filamentary structures in all the cases. These structures arise due to the Weibel instability. This can be understood as two streams, the hot-electrons stream, which is generated at the laser-plasma interface and the cold return plasma stream, interacting with each other.

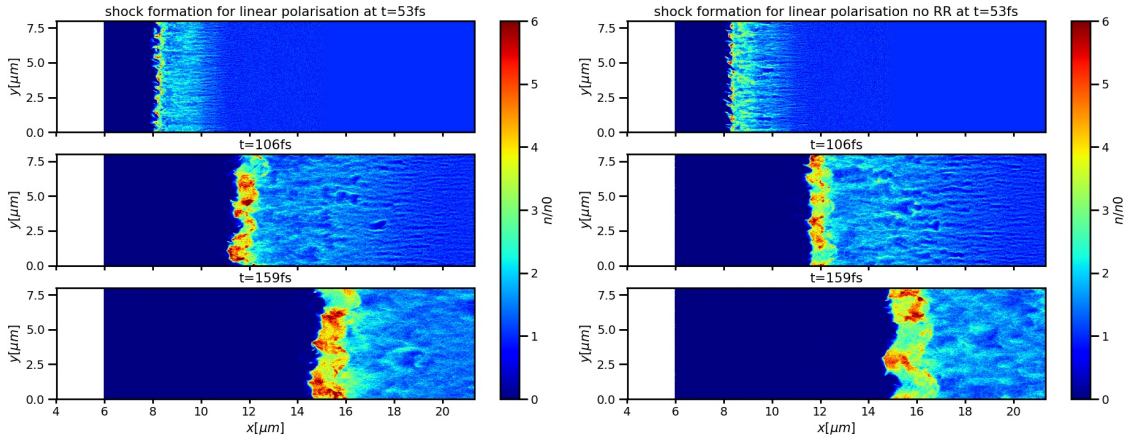

(a) including radiation reaction (b) without radiation reaction

Fig. 3: plasma density (normalized by initial density) at different times for linear polarisation density $420n_c$, $a_0 = 400$

In the circular polarised case the shock formation is less pronounced than in the linear case. The linearly polarised laser has a deeper penetration in the target and causes stronger heating of the target which helps in launching a shock with larger width. In the case of circularly polarised light, the heating of the electrons is less stronger than the linearly polarised case. Consequently, the shock formation occurs but with a smaller width. This can have an impact on the laser scattering since the analytical calculations do not take into account the shock formation. It's expected that at a fixed density the linearly polarised light can produce more positrons and consequently can gets scattered strongly.

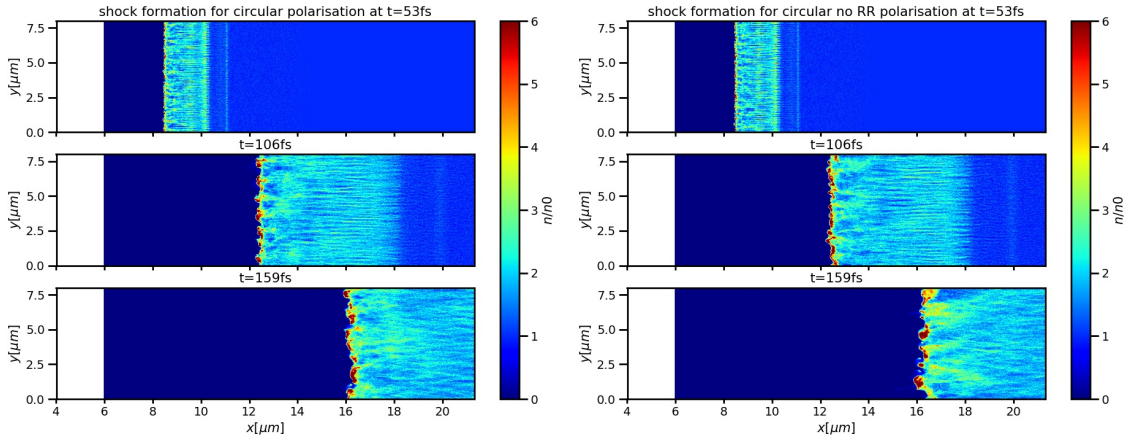

(a) including radiation reaction (b) without radiation reaction

Fig. 4: plasma density (normalized by initial density) at different times for circular polarisation density $420n_c$, $a_0 = 400$

4.2 Scattering

To further understand the development of the instability, PIC simulations with different densities and laser pulse are carried out. These simulations evaluate the dependency of the scattering on pair production and polarisation. To examine the dependence of $k_\perp$ on the scattering, simulations with a Gaussian pulse in time and space were also launched. Also, the impact of the polarisations on the scattering was analysed.

4.2.1 Pair production

In Fig.5 the number of created positrons over the time can be seen. It shows that in most cases the number of positrons reaches a maximum value and decays after. The positron production is higher at higher plasma densities. For the Gaussian laser pulse simulations, one sees less number of positrons generated, hence one can expect lower scattering.

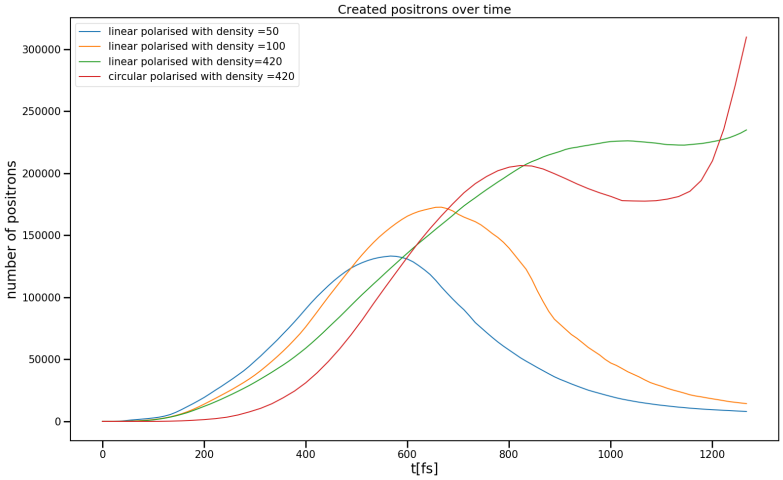

(a) all the planar wave cases e.g. for linear polarisation the densities 50, 100, 420 n_c all with $a_0 = 400$ and for circular polarisation $n_0 = 420n_c$ and $a_0 = 400$

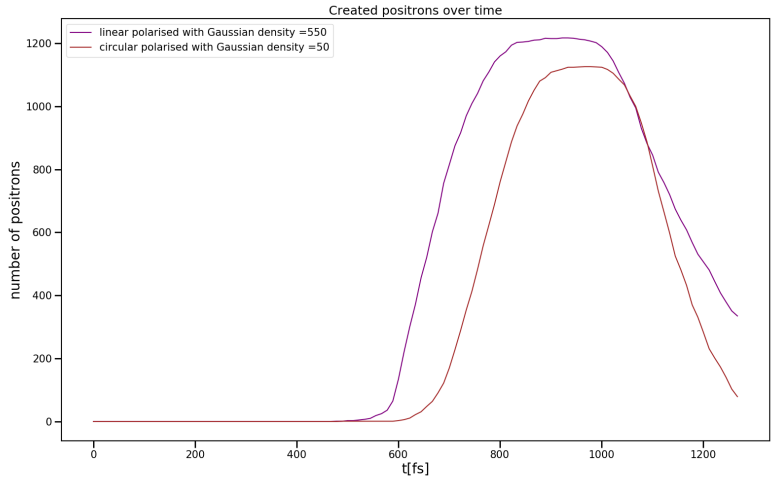

(b) Gaussian laser pulse with $n_0 = 550n_c$ and $a_0 = 420$ for linear polarisation and $n_0 = 50n_c$ and $a_0 = 350$ for circular polarisation

Fig. 5: number of created positrons for the different settings

4.2.2 Linear laser pulse at low plasma density

To examine the development of the laser scattering, we study the spatial spectra of the plasma field (E_x) and laser field (E_y) over time. We take Fourier transforms of the plasma field both over x and y directions. This can be seen in the Figs.6 - 11. These figures were generated by calculating $\int_0^{L_{x/y}} \int_0^{L_{x/y}} E_{x/y}(x,y) e^{ik\cdot x/y} dxdy$ and displaying it at different times. The following simulation results clearly shows the effect of the pair-production on the laser scattering with and without radiation reaction Figs.7 and 9. Figs. 6 and 7 show the spatial growth for the different fields in case of linear polarisation with and without radiation reaction force.

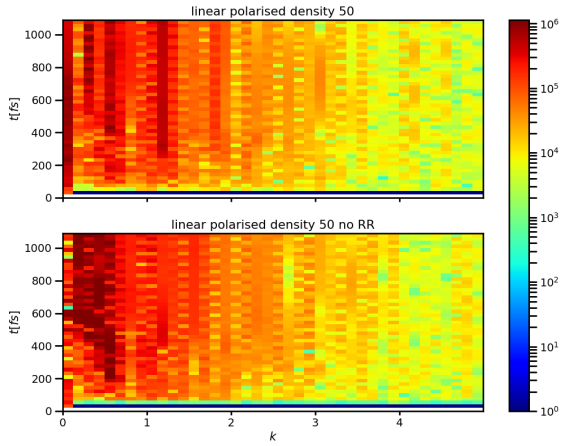

Fig. 6: Spatial spectra (Fourier transformed in y direction) of the plasma field for linear polarisation with and without RR. Both cases have an $a_0 = 400$ and a density of $n_e = 50 n_c$.

Fourier transformed of the plasma electric field in y shows the appearance of few peaks at k_0, where k_0 is wavevector of the incident laser pulse. One can see that the plasma longitudinal field E_x has a broad k-spectrum and shows few harmonics at $k_0 < 1$ and $k_0 > 1$ (corresponding to the plasma wavevector $k_p > 1$) with the radiation reaction force. While without the radiation reaction force, one sees the

k-spectrum is limited to $k_0 < 1$. This implies a stronger modulation of the laser envelope but also the lack of a stronger plasma wakefield generation, in sync with theoretical assumptions see 3.58. Hence, comparing these two figures one can see that the radiation reaction force is causing the generation of the plasma wakefield. One may also see that in the k-spectrum for $k_0 < 1$, shows step like structures in both cases, and this can be connected with the combined effects of the relativistic plasma oscillations or the pair-production.

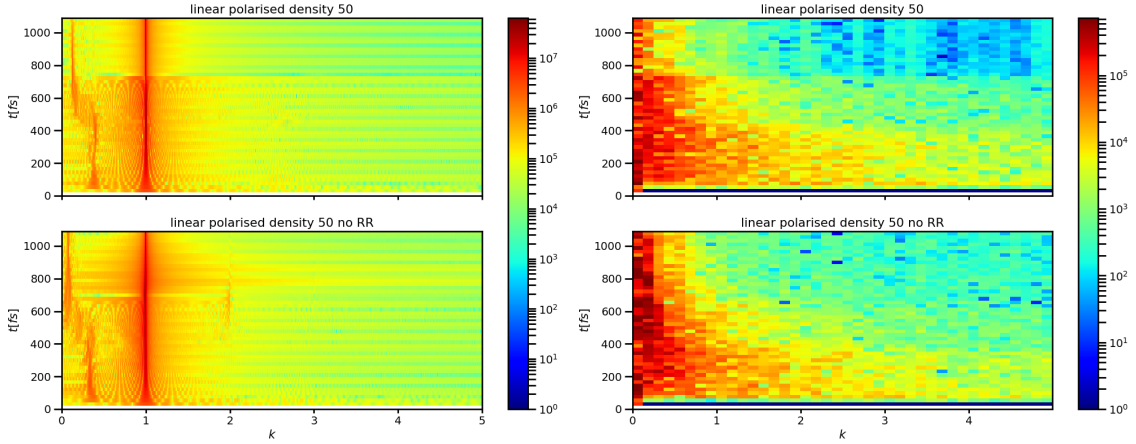

(a) Fourier transformed in x direction (b) Fourier transformed in y direction

Fig. 7: Spatial spectra of the laser field for linear polarisation with and without RR. Both cases have an $a_0 = 400$ and a density of $n_e = 50n_c$.

Fig. 7 shows the Fourier transformed (in x and y directions) laser field. The line $k_0 = 1$ corresponds to the laser wavevector, the other visible line at $k_0 \approx 0.5$ corresponds to the scattering of the laser pulse. At later time, this line approaches the $k_0 = 0$ in the case of no RR force while it stays around $k_0 \approx 0.25$ in the case of radiation reaction force. This implies a stronger modulation of the laser pulse envelope at $\lambda = 2\lambda_0$ wavelength suggesting the red-shifting of the carrier-envelope frequency. Fig. 7b shows the Fourier transformed electric field in y-direction. This is most important result of the thesis and it shows higher scattering due to pair-production

at $k \leq k_0$. This qualitatively confirms the theoretical predictions presented in the Sec. 3. Later on we show a result where we have included the radiation reaction force but not the pair-production, Figs. 12 - 14.

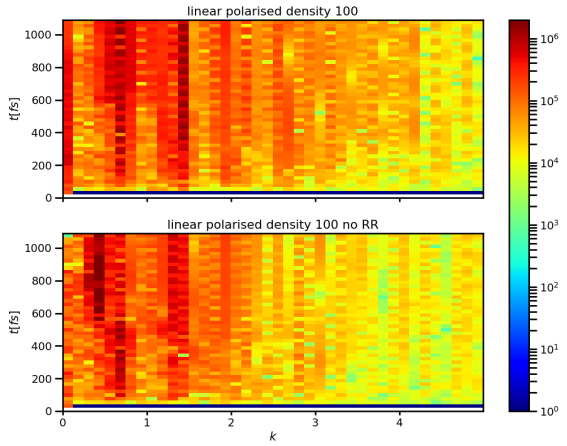

Fig. 8: Spatial spectra (Fourier transformed in y direction) of the plasma field for linear polarisation with and without RR. Both cases have an $a_0 = 400$ and a density of $n_e = 100 n_c$.

At higher densities, $n_0 = 100\, n_c$ shown in Fig.8, we continue to see the same trend as before. In this case the effect of the radiation reaction is stronger than at density $n_0 = 50 n_c$. The k-spectrum of the plasma field in Fig. 8 is visibly broader in case of radiation reaction than in case of no radiation reaction force. In the case of radiation reaction force, the plasma longitudinal electric field seem to show a peak at the backward Raman scattering wavenumber. The step-like structures in this case are presumably due to the pair-production. Fig. 9 shows again the laser field. Here also the previous trends can be further seen. The scattering of the laser pulse is again stronger in the case of pair-production compared to the no radiation reaction force case. The k-spectrum in the case of radiation reaction force (Fourier transformed in x) shows peaks both at $k_0 = 1$ and at $k_0 \approx 0.5$ but this time the line approaches $k_0 \approx 0.25$ in both cases. The Fourier transformed (in y direction) laser field shows a

visibly broader compared to the case of no radiation reaction force.

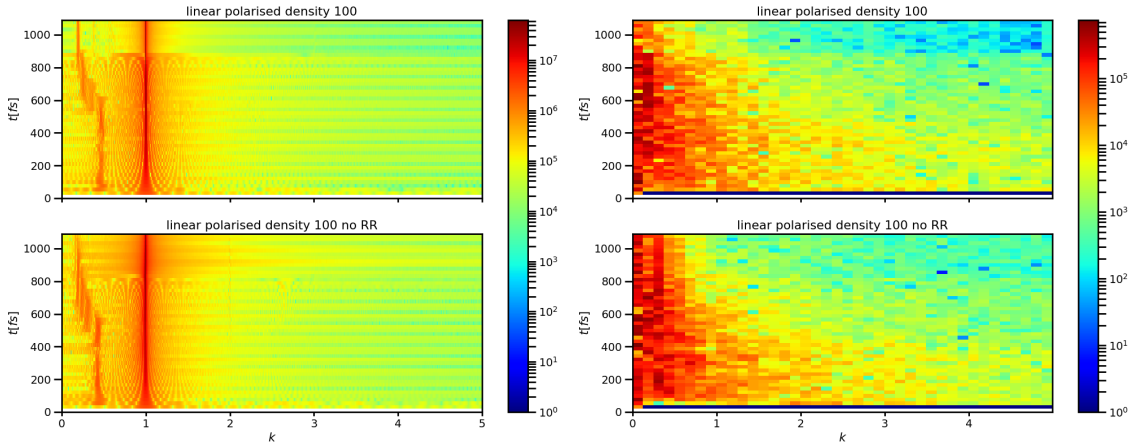

(a) Fourier transformed in x direction (b) Fourier transformed in y direction

Fig. 9: Spatial spectra of the laser field for linear polarisation with and without RR. Both cases have an $a_0 = 400$ and a density of $n_e = 100n_c$.

4.2.3 Gaussian circular laser pulse at lower density

Here the same circularly Gaussian laser pulse was used, but for $a_0 = 350$ and density $50n_c$. In this case, the plasma field spectra Fig. 10 shows absence of well-defined harmonics at different k as in the previous section. The Fourier transformed laser field shown in Fig. 11a again a secondary structure around $k \approx 0.5$ that tends to lower k values at later times. Although the scattering is stronger than in the previous Gaussian case, Fig. 18, it is not as strong as in the cases with $a_0 = 400$ and $n_0 = 420n_c$ as seen in Figs. 14 and 16 or $a_0 = 400$ and $n_0 = 50n_c$ in Fig. 7. Which again demonstrates the effect of $k_\perp$. For this case also the difference between radiation reaction and no radiation reaction is not visibly clear.

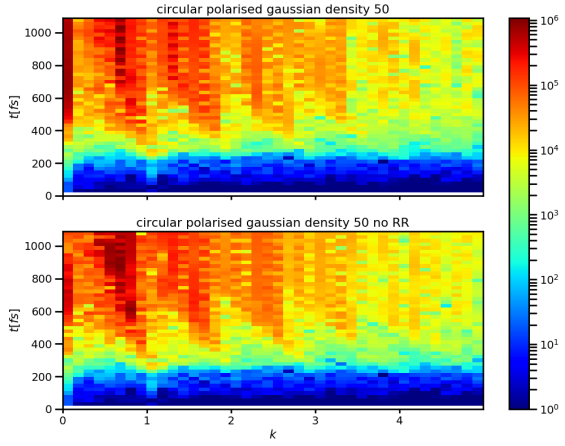

Fig. 10: Spatial spectra (Fourier transformed over y) of the plasma field for a circular polarised Gaussian laser pulse with and without RR. Both cases have an $a_0 = 350$ and a density of $n_e = 50n_c$.

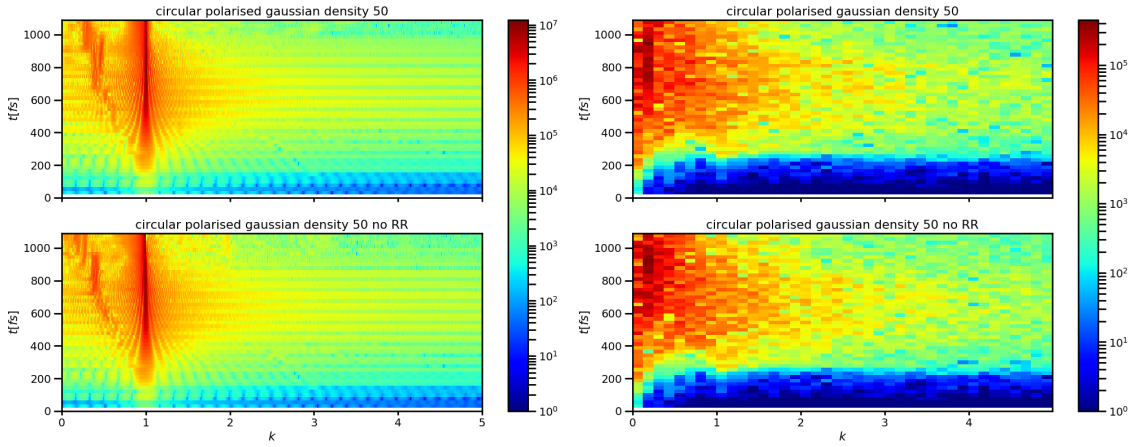

(a) Fourier transformed in x direction (b) Fourier transformed in y direction

Fig. 11: Spatial spectra of the laser field for a circular polarised Gaussian laser puls with and without RR. Both cases have an $a_0 = 350$ and a density of $n_e = 50n_c$.

4.2.4 Linear laser pulse with RR/PP

The next simulation we considered was a planar linear polarised laser pulse with $a_0 = 400$ propagating through a plasma with density $420n_c$. This was conducted to see the changes on including the radiation reaction force but no pair-production.

The Fourier transformed of the plasma electric field in y Fig.12 shows some

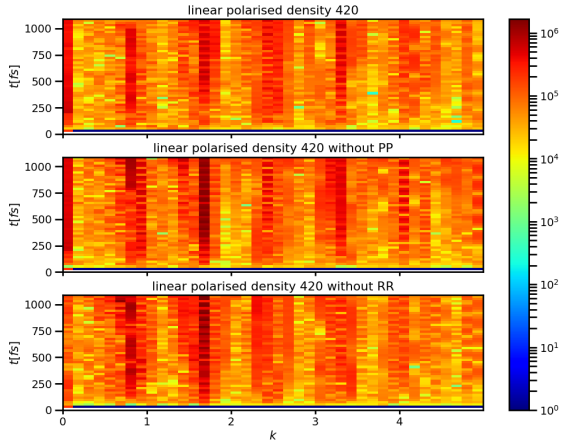

Fig. 12: Spatial spectra (Fourier transformed over y) of the plasma field for linear polarisation with and without RR and PP. All three cases have an $a_0 = 400$ and a density of $n_e = 420n_c$.

differences. The line around $k \approx 1.75$ seems to be stronger in case of radiation reaction force but without including the pair production. This line is weaker without accounting for the radiation reaction and pair-production. This line disappears on accounting for both effects. This can be understood as follows: in the presence of the radiation reaction this backscattering gets stronger due to the plasma layer compression (see next figure) by the laser pulse. On accounting for the pair-production, this layer looses its energy due to quasi-neutrality and energy being diverted to the pair-production, and hence it gets weakened.

To verify the assumption of the redistribution of the energy, we can take a look

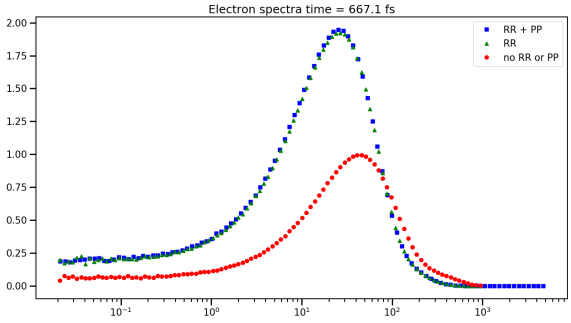

(a) Electron

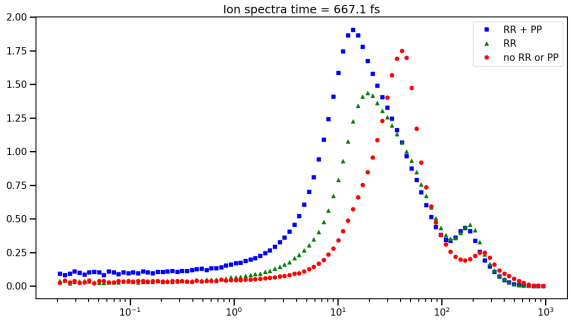

(b) Ion

Fig. 13: Energy spectra for time 667.1 fs

at the electron and ion spectra for this cases. This can be seen in Fig.13. For the electrons there is no difference in the energy spectrum in both cases. In the ion energy spectra there is a visible change. In the case of pair production, the maximum is at a lower value than with only radiation reaction. This shift in the energy resulted from the destruction of the plasma density compression and hence the suppression of the double layer.

In the spatial spectra of the laser field, Fig.14, we can't see a visible difference in both cases. In this case the scattering of the laser pulse occurs at $k_0 \approx 0.7$ and a second structure appearing in all three cases at $k_0 \approx 1$ can be seen. Most of the scattering in Fig.14b is restricted to $k \leq k_0$ and no visible change between the different cases

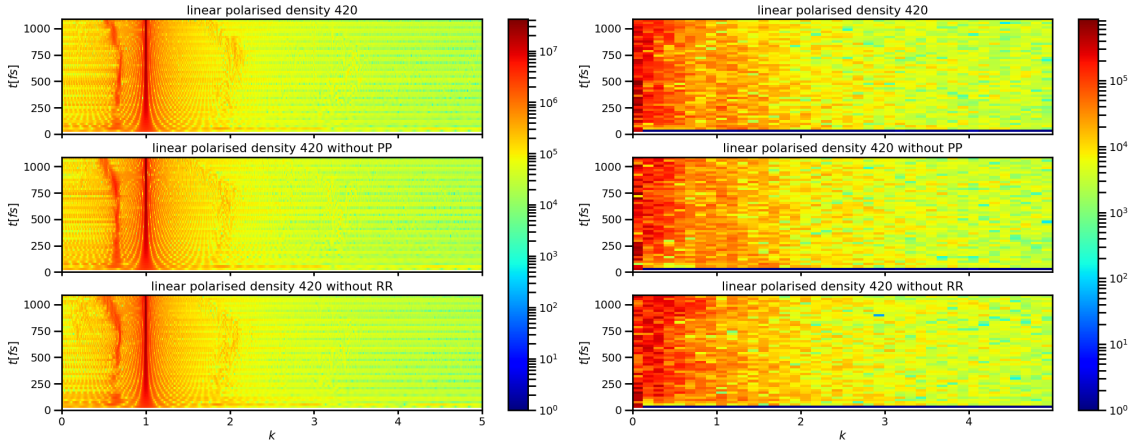

(a) Fourier transformed in x direction (b) Fourier transformed in y direction

Fig. 14: Spatial spectra of the laser field for linear polarisation with and without RR and PP. All three cases have an $a_0 = 400$ and a density of $n_e = 420 n_c$.

can be seen. Thus at higher densities, the effect due to pair-production on the laser scattering in transverse direction is negligible though in the propagation direction we do see a quantitative shift towards $k \approx 1$ of the secondary structure.

4.2.5 Circular laser pulse

Here a planar circular polarised laser pulse with $a_0 = 400$ and density $420 n_c$ was chosen to make the difference between the polarisation dependence on the laser scattering apparent.

The plasma field in Fig.15 again shows similar structure as before Fig.12. However, the line at $k \approx 1$ seems to be the strongest. The Fourier transformed laser field Fig.16 shows the scattered line due to secondary structure appears again at approximately ≈ 0.7 as in the linearly polarised case. Fourier transformed (in y-direction) laser field shows a very minute difference between the cases of no radiation reaction and pair-production. Although, there is slight broadening of the k-spectrum in the case of pair-production. This suggest that pair-production indeed has some influence on

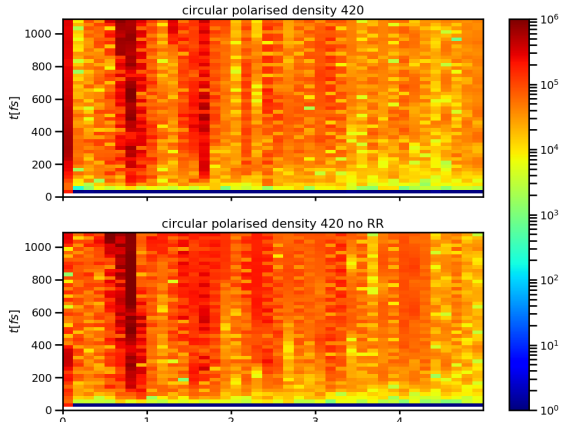

Fig. 15: Spatial spectra (Fourier transformed over y) of the plasma field for circular polarisation with and without RR. Both cases have an $a_0 = 400$ and a density of $n_e = 420 n_c$.

the laser scattering even in high plasma densities case. Overall the scattering in due to circular polarisation is less than due to linear polarisation, which is to be expected since for given λ and I the a_0 value in the linear case is a factor of $\sqrt{2}$ bigger than in the circular case.

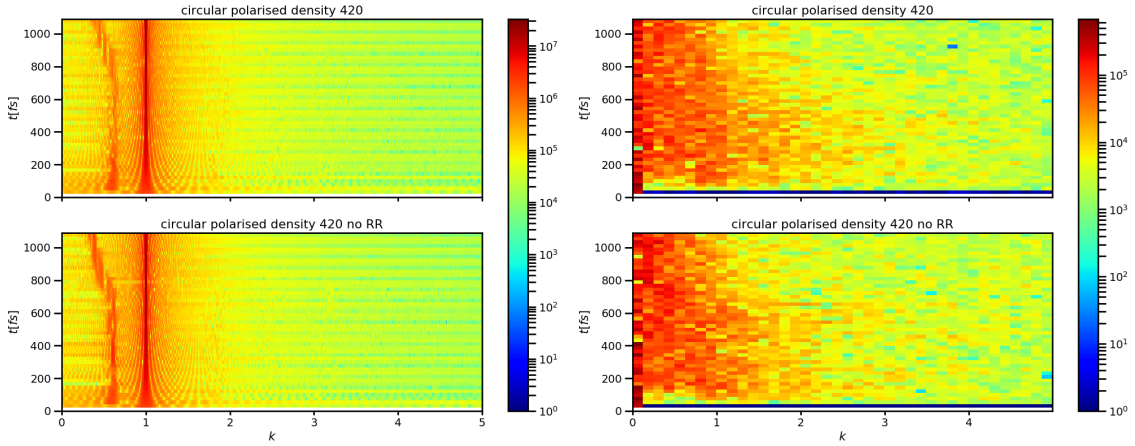

(a) Fourier transformed in x direction (b) Fourier transformed in y direction

Fig. 16: Spatial spectra of the laser field for circular polarisation with and without RR. Both cases have an $a_0 = 400$ and a density of $n_e = 420 n_c$.

4.2.6 Gaussian linear laser pulse at high density

To examine the effects of a finite $k_\perp$ we chose a Gaussian envelope in time and space for a linear polarised laser pulse with $a_0 = 420$ propagating through a plasma with density $550n_c$. In the plasma field show in Fig.17 one see similar behaviour as before

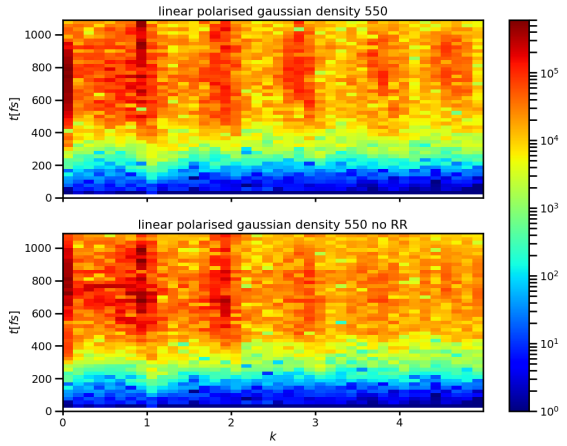

Fig. 17: Spatial spectra (Fourier transformed over y) of the plasma field for a linear polarised Gaussian laser pulse with and without RR. Both cases have an $a_0 = 420$ and a density of $n_e = 550n_c$.

and the structures at higher k seems to be weaker in the case of pair-production. In this case, the lines at different k are integer multiples of k_0, whereas in the planar linear case, see Fig.12, the harmonics can be found at slightly lower values. The Fourier transformed laser field shown in Fig.18 depicts only one stronger line at $k_0 = 1$, corresponding to the laser pulse. Which means that for this case there isn't as a secondary structure formation occurring. The Fourier transformed (in y direction) laser field field shown in Fig.18b, shows larger scattering for a brief period of time (between 600 and 800 fs) at smaller $k \approx 0.2$ number for pair-production case. Though the scattering at larger k numbers is almost same. This is also expected from the theory. The scattering is stronger when the pair-productions is higher but the finite $k_\perp$ reduces the growth of the perturbation.

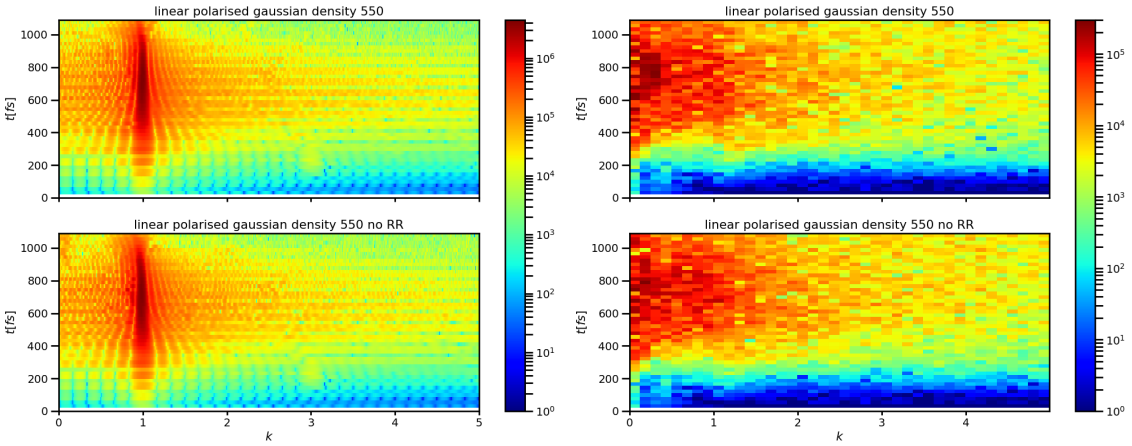

(a) Fourier transformed in x direction (b) Fourier transformed in y direction

Fig. 18: Spatial spectra of the laser field for a linear polarised Gaussian laser puls with and without RR. Both cases have an $a_0 = 400$ and a density of $n_e = 550 n_c$.

5 Conclusion

Based on the simulation results presented before one can see that scattering in the transverse direction due to pair-production is dominant in low plasma density regime, Fig.24. At higher plasma density the scattering in transverse direction is same with and without the radiation reaction and pair-production. This is due to the fact that pair-production saturate at high plasma densities and consequently the scattering shows no difference with and without the radiation reaction force and pair-production. The scattering due to pair-production at lower density is important since it suggests that there can be a higher scattering of the laser pulse hindering the development of the electromagnetic cascade induced by two laser pulses. Also, the results with Gaussian spatial profiles confirm the theoretical prediction that even though the pair-production is sufficient the laser scattering due to pair-production is same as without the pair-production case at early time. This is due to the finite $k_\perp$ that reduces the growth rate of the instability and requires longer interaction time for instability to show its signature, see 3.58.

6 Outlook

The results look promising for studying the scattering in low-plasma density regimes. One needs to do more simulation in this regime and especially with the circular polarised laser pulse. PIC simulations in this regime are resource demanding and due to higher plasma density compression occurring at lower plasma densities, they take longer time to finish, and this is the reason they have not been included in the thesis yet. Moreover, we need to repeat these simulations for electron-positron plasmas to see if it has an impact on the electromagnetic cascade initiated by two counter-propagating laser pulses.

References

[1] https://www.eli-np.ro/documents/press_releases/Comunicat_Presa_Eng_10PW.pdf, (accessed September 4, 2019).

[2] M. Dunne, "A high power laser fusion facility for europe," *Nature Physics*, vol. 2, 01 2006.

[3] J. W. Dawson, J. Crane, M. J. Messerly, M. A. Prantil, P. H. Pax, A. K. Sridharan, G. S. Allen, R. Drachenberg, H. Phan, J. Heebner, C. A. Ebbers, R. J. Beach, E. P. Hartouni, C. Siders, T. M. Spinka, C. P. J. Barty, A. Bayramian, C. Haefner, F. Albert, and R. E. Bonanno, "High average power lasers for future particle accelerators," *AIP Conference Proceedings*, vol. 1507, pp. 147–153, 12 2012.

[4] G. Harry, P. Fritschel, W. Folkner, D. Shaddock, and E. Sterl Phinney, "The big bang observer: High laser power for gravitational wave astrophysics," 05 2007.

[5] S. Kalmykov and G. Shvets, "Compression of laser radiation in plasmas using electromagnetic cascading," *Physical review letters*, vol. 94, p. 235001, 06 2005.

[6] M. Jirka, O. Klimo, M. Vranic, S. Weber, and G. Korn, "Qed cascade with 10 pw-class lasers," *Scientific Reports*, vol. 7, p. 15302, 12 2017.

[7] https://www.researchgate.net/figure/History-of-laser-intensity-showing-the-different-laser-matter-interaction-periods-Over_fig2_231066372, (accessed August 29, 2019).

[8] A. Di Piazza, C. Müller, K. Hatsagortsyan, and C. H. Keitel, "Extremely high-intensity laser interactions with fundamental quantum systems," *Reviews of*

Modern Physics, vol. 84, 11 2011.

[9] Y. Hadad, L. Labun, J. Rafelski, N. Elkina, C. Klier, and H. Ruhl, "Effects of radiation-reaction in relativistic laser acceleration," *Physical Review D*, vol. 82, 05 2010.

[10] A. R Bell and J. Kirk, "Possibility of prolific pair production with high-power lasers," *Physical review letters*, vol. 101, p. 200403, 12 2008.

[11] Z. Bian and T. M. Antonsen, "Ionization instabilities of an electromagnetic wave propagating in a tenuous gas," *Phys. Plasmas*, vol. 8, p. 3183, 2001.

[12] E. Efimenko and A. Kim, "Strongly coupled regime of ionization-induced scattering in ultrashort laser-matter interactions," *Physical review. E, Statistical, nonlinear, and soft matter physics*, vol. 84, p. 036408, 09 2011.

[13] W. Kruer, *The Physics Of Laser Plasma Interactions*. Westview Press, 2003.

[14] P. Gibbon, *Short Pulse Laser Interactions with Matter: An Introduction*. World Scientific Publication Company, 2005.

[15] J. Derouillat, A. Beck, F. Pérez, T. Vinci, M. Chiaramello, A. Grassi, M. Flé, G. Bouchard, I. Plotnikov, N. Aunai, J. Dargent, C. Riconda, and M. Grech, "Smilei : A collaborative, open-source, multi-purpose particle-in-cell code for plasma simulation," *Computer Physics Communications*, vol. 222, pp. 351 – 373, 2018.

[16] N. M. Larsgaard. `https://folk.idi.ntnu.no/elster/master-studs/larsgaard/larsgaard-master.pdf`, (accessed September 2, 2019).

Appendices

A PIC algorithm

PIC is a method which was developed in the 1960s. For this technique the distribution function is represented by many discrete macro particles ("quasi particles") each carrying a specific charge (q_i) and mass (m_i). This stands in contrast to the Vlasov equation 3.3 which takes the distribution as a whole. The density is in case of a PIC simulation assumed to be:

$$\rho(x) = \sum q_i S(x_i - x)\delta(p - p_i), \tag{A.1}$$

where $S(x_i - x)$ describes the form of the macro particles. The shape functions used in SMILEI can be found in Appendix A of [15].
Using the relativistic equation of motion/Lorentz equation

$$\frac{\partial u_i}{\partial t} = r_s(E_i + \frac{u_i}{\gamma_i} \times B_i), \tag{A.2}$$

where $r_s = q_s/m_s$ (for species s) and $u_i = p_i/m_s$ the quasi-particle reduced momentum as well as the fields

$$E_i = \int dx S(x_i - x)E(x), \tag{A.3}$$

$$B_i = \int dx S(x_i - x)B(x), \tag{A.4}$$

we can calculate the next time-step. To get the next time-step out of the equation motion the leap frog algorithm is used. The new particle momentum and position is

then calculated according to :

$$\begin{aligned} u_i^{(n+\frac{1}{2})} &= u_i^{(n-\frac{1}{2})} + r_s \Delta t \left(E_i^{(n)} + \frac{v_i^{(n+\frac{1}{2})} + v_i^{(n-\frac{1}{2})}}{2} \times B_i^{(n)} \right) \\ x_i^{(n+1)} &= x_i^{(n)} + \frac{u_i^{(n+\frac{1}{2})}}{\gamma_i} \Delta t, \end{aligned} \tag{A.5}$$

whereas Δt is the duration of a time-step and n denotes the time-step. The current density J is calculated in similar manner by using the charge conservation . With the help of the Maxwells equations the fields can than be determined. Thus the necessary components are computed for this time-step and the algorithm starts anew for the next time-step.

```
1: Initialize(field, particles)
2: while t < t_max do
    3: Calculate particles contribution to field
    4: Solve the field
    5: Update particle speed
    6: Update particle position
    7: Write plot files
```

Fig. 19: PIC loop [16]

Erklärung

Ich versichere, dass ich diese Arbeit selbstständig verfasst und keine anderen als die angegebenen Quellen und Hilfsmittel benutzt habe.

Heidelberg, den 9. September 2019